



# Geosynthetic-reinforced soils above voids: Observation of soil and geosynthetic deformation mechanisms

T.S. da Silva Burke<sup>a,1,\*</sup>, M.Z.E.B. Elshafie<sup>b</sup>

<sup>a</sup> Department of Civil Engineering, University of Pretoria, South Africa

<sup>b</sup> Department of Civil & Architectural Engineering, College of Engineering, Qatar University, Doha, Qatar

## ARTICLE INFO

### Keywords:

Geosynthetic-reinforcement  
Void spanning  
Centrifuge  
PIV

## ABSTRACT

Understanding how a geosynthetic-reinforced soil deforms in response to the formation of an underlying void is crucial to provide appropriate designs of these systems. Centrifuge models employing a trapdoor to simulate the void formation below a geosynthetic-reinforced sand were conducted to investigate the behaviour in a controlled environment at realistic stress levels. The plane-strain models allowed visual observations of the deformation mechanisms using Particle Image Velocimetry (PIV). These observations were used to validate assumptions about the geosynthetic behaviour made in current design recommendations, and address limitations related to the fill behaviour. Soil expansion was observed to be confined to a parabolic zone above the void related to the soil dilatancy, rather than with a single, unique coefficient of expansion. The zone of subsidence was characterised by an initial vertical prism with a funnel to the surface, with the surface settlement profile better described by a Gaussian distribution rather than the parabolic profile used historically. Detailed interpretation of the centrifuge tests has given new insight into the soil and geosynthetic behaviour relevant to how these systems deform in practice. This paves the way for more efficient design recommendations and consequently will facilitate better predictions of geosynthetic-reinforced soil behaviour above voids.

## 1. Introduction

Geosynthetic-reinforced soils are used in the construction of transportation networks over areas with high potential for void formation such as karstic geologies or undermined areas where problems may be caused by sinkholes or collapse of underground mine workings, and potential impact is widespread and unpredictable. Financial losses in the case of failure can be large, and considerable cost savings are possible through the incorporation of preventative measures (Galve et al., 2012; Cooper and Calow, 1998; SANS, 1936-1, 2012).

Geosynthetic-reinforcement is used to reduce the risk of catastrophic collapse and allow time for remediation (in the case of large voids), or, for small voids, to limit differential settlement of the surface and thus maintain the serviceability of the infrastructure (Jones and Cooper, 2005). An effectively designed reinforcement will span the void and support the imposed soil and traffic loads without excessive deflection or rupture. The geosynthetic deformation propagates through the soil to the surface where it could have a critical impact on the infrastructure serviceability.

Applications of the design procedure require an accurate

understanding of the geosynthetic and soil fill behaviour to ensure that the geometric aspects are appropriately applied. The current assumptions regarding the way this deformation at the geosynthetic level is propagated through the soil to the surface vary widely in existing design methodologies. Experimental validation of the deformation mechanisms in the geosynthetic and soil remain limited. In this research work, physical model tests of the behaviour of basal-reinforced granular fills over voids were conducted in a geotechnical centrifuge to investigate these mechanisms and contribute to the understanding of this behaviour.

## 2. Design procedures

When a void forms below a geosynthetic-reinforced soil, the geosynthetic deflects into the void. The load transfer is achieved via soil arching and the development of tension in the geosynthetic as it is stretched, known as the membrane effect. Soil arching theory is used to determine the applied stress on the geosynthetic; further discussion on this is given in da Silva Burke and Elshafie (2020b).

A geometric consideration of the soil and geosynthetic behaviour is

\* Corresponding author.

E-mail address: [talia.burke@up.ac.za](mailto:talia.burke@up.ac.za) (T.S. da Silva Burke).

<sup>1</sup> Formerly Department of Engineering, University of Cambridge, Trumpington Street, Cambridge, CB2 1PZ, UK.

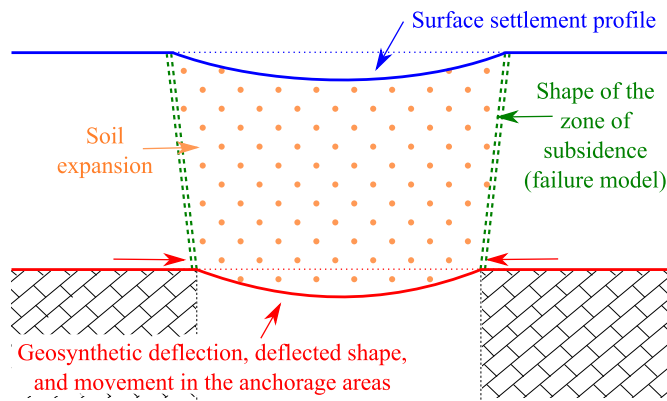


Fig. 1. Geometric aspects of behaviour of reinforced soils above voids to be considered in design.

used to relate the critical deflection or deflection ratio at the surface to the maximum allowable geosynthetic deflection above the void, based on an assumed deflected shape of the geosynthetic. The applied stress and deflected shape are used in combination to design the required strength and stiffness of the geosynthetic.

The key aim of any design with geosynthetic-reinforcements over voids is to limit the deflection of the soil at some height above the geosynthetic layer; a generic procedure for this design process is presented in da Silva and Elshafie (2018). Understanding the mechanism of the soil deformation and how the settlement at the surface can be related to the geosynthetic deflection is thus of fundamental importance. There are four components of the geometric behaviour to be considered, described below and represented in Fig. 1.

- (i) Geosynthetic behaviour, including maximum deflection, deflected shape, and movement in the anchorage area;
- (ii) Shape of the zone of subsidence, i.e. the failure model or width of the affected soil region;
- (iii) Soil expansion, expected to be related to dilation in a granular material, and
- (iv) Soil surface settlement profile.

A review of the membrane effect and the existing design methods is given in this section. This is followed by a review of further research conducted into the nature of the geosynthetic and fill behaviour, and a summary of the limitations of existing research and remaining questions.

### 2.1. Membrane effect

The membrane effect refers to the ability of a geosynthetic sheet to deflect and absorb forces initially perpendicular to its surface through tension (Gourc and Villard, 2000). This requires a differential displacement; the membrane effect can thus only be used where a minimum amount of deformation is possible.

The geosynthetic deflection profile and resultant tension and strain developed in the geosynthetic, depends on the applied stress distribution and orientation of the stress on the deflected geosynthetic (Villard and Briançon, 2008; van Eekelen and Bezuijen, 2012). If the applied stress across the void remains vertical, a constant horizontal tension,  $T_0$ ,

is developed in the geosynthetic, and the deflection profile is equivalent to the bending moment of the stress distribution divided by  $T_0$ . If the stress is applied normal to the deflected geosynthetic, a constant tension and strain is developed in the geosynthetic which results in a constant radius of curvature,  $\rho$ . Table 1 shows a summary of the deflection profiles in the most common loading cases considered, for a void width of  $B$ .

To give an indication of the effect of the stress distribution and orientation assumptions, the deflection and strain profiles based on an average stress of  $p = 25$  kPa, void width of  $B = 2$  m, and geosynthetic stiffness of  $J = 1000$  kN/m are shown in Fig. 2. In the figure, it can be seen that the circular and parabolic deflection profiles are approximately equivalent, and thus the stress orientation, i.e. normal or vertical, makes little difference to the deflection profile. The assumption of a vertical orientation results in a higher maximum strain than a normal orientation of stresses where a constant strain is developed, although the difference is marginal.

The assumption of a triangular stress distribution results in the highest deflection and strain in the geosynthetic; this is as expected as the majority of the load is further from the supported edge. Conversely, the assumption of an inverse-triangular distribution results in the lowest values.

These variations are important to understand as it affects whether assumptions made in the design process are conservative or unconservative, and has implications for the analysis of the test results reported in this paper and recommendations for further use.

### 2.2. Existing design methods

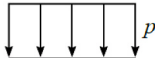


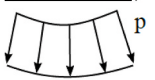
There are three primary analytical design methods used in practice for the evaluation of geosynthetic-reinforced soils above voids; these are:

- British Standard BS8006: ‘Code of practice for strengthened reinforced soils and other fills’ (BS8006, 2010);
- RAFAEL: a design method developed from the experimental results of the French research program (Blivet et al., 2002; Villard et al., 2000); and
- EBGeo: German design guideline ‘Recommendations for Design and Analysis of Earth Structures using Geosynthetic Reinforcements’ (EBGeo, 2010).

The assumed deformation behaviour of the soil and geosynthetic in each of these design methods is shown schematically in Fig. 3; the following items are noted:

- (i) Geosynthetic behaviour: all of the methods assume that the deflected geosynthetic shape is parabolic (i.e. vertical, uniform load distribution) and that the geosynthetic is fixed at the edge of the voids.
- (ii) Soil surface settlement: all of the methods assume that the soil surface settlement is parabolic, forming paraboloids of revolution with the deflected geosynthetic profile.
- (iii) Shape of zone of subsidence: RAFAEL assumes the formation of a cylindrical failure zone, whilst EBGeo assumes the formation of a narrow truncated cone with an angle of draw,  $\theta_D$ , of  $85^\circ$ . BS8006 assumes a wide truncated cone with  $\theta_D$  equal to the angle of friction of the fill material.
- (iv) Soil expansion: BS8006 ignores any soil expansion, whilst EBGeo

**Table 1**  
Calculations of the deflection and strain of geosynthetic under various applied loads.

Load distribution & orientation	Deflected shape	Deflection profile, $z(x)$	Maximum deflection, $d$	Approx. max. strain, $\epsilon_{max}$
Uniform, vertical		Parabolic	$-\frac{pB^2}{8T_0}$	$\frac{8}{3} \left(\frac{d}{B}\right)^2$
Inverse triangular, vertical		Cubic	$-\frac{pB^2}{24T_0} + \frac{px^3}{3BT_0}$	$\frac{18}{5} \left(\frac{d}{B}\right)^2$
Triangular, vertical		Cubic & quadratic	$-\frac{pB^2}{12T_0} + \frac{px^2}{2T_0} - \frac{px^3}{3BT_0}$	$\frac{12}{5} \left(\frac{d}{B}\right)^2$
Uniform, normal		Circular	$-\frac{\sqrt{\rho^2 - x^2} + \sqrt{\rho^2 - B^2/4}}$	$\frac{8}{3} \left(\frac{d}{B}\right)^2$

and RAFAEL assume a constant soil expansion in the deformed region with an empirical value relating the deflected geosynthetic and soil surface volume varying depending on the fill material.

2.3. Further research and developments

2.3.1. Geosynthetic behaviour

Various studies have been conducted in an attempt to identify the

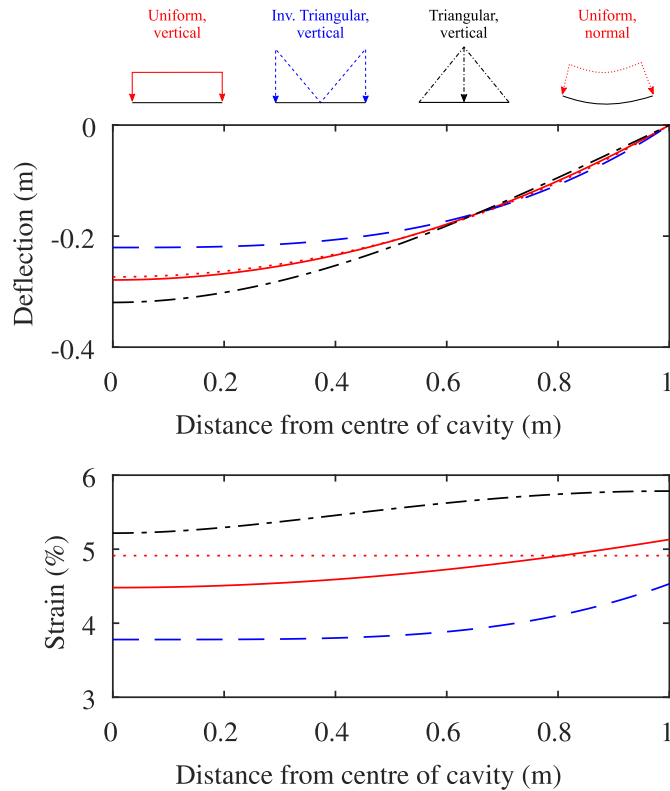


**Fig. 2.** Effect of assumed stress distributions and orientations on geosynthetic deflection and strain profiles; calculated with  $p_{ave} = 25$  kPa,  $B = 2$  m, and  $J = 1000$  kN/m.

deflected shape of a geosynthetic over a void and the strains induced, and thus infer the stress distribution across the geosynthetic. Additionally, investigations into the effect of displacement in the anchorage areas have been conducted with an attempt to estimate these displacements.

An update to the RAFAEL design method has been provided by Villard and Briançon (2008) based on full-scale tests described by Briançon et al. (2005) to include the effects of geosynthetic stretching and slippage in the anchorage area (Briançon and Villard, 2008; Villard and Briançon, 2008). This results in an increase in the geosynthetic deflection, and lowering of the tension developed in the geosynthetic. Huckert et al. (2016) highlight that for typical soil-geosynthetic interface friction values, these effects can lead to a doubling of the tensile stiffness required to meet design surface deflection criterion.

Laboratory scale model studies on geosynthetic-reinforced piled embankments were conducted by van Eekelen and Bezuijen (2012) and van Eekelen et al. (2012a, b); piled embankments evaluated in plane-strain are expected to behave similarly to infinitely long voids. These results showed that the measured deflection profile of the geosynthetic between the pile caps most closely followed a cubic deflection profile, with an inverse-triangular stress distribution. Bezuijen and van Eekelen (2014) provided a 2D numerical validation for the use of an inverse-triangular load distribution by considering the Terzaghi load transfer model from a series of equivalent trapdoors across a void.

Huckert et al. (2014, 2016) conducted full scale experiments of geosynthetic-reinforced granular embankments over circular voids. The reported geosynthetic shape was parabolic in these tests which infers a uniform load distribution (see Table 5). Numerical modelling was used in Huckert et al. (2014) to deduce the load-distribution; an inverse-triangular shape was found for the smaller cavity, and uniform for the larger cavity. Monitoring of geosynthetic strains in the experiments showed that strains developed in the anchorage area for a distance equivalent to the void diameter. The experimentally measured maximum deflection and strains in the anchorage area measured in the experiments matched well with a comparison to the analytical method of Villard and Briançon (2008). Design of geosynthetic-reinforced embankments over voids should therefore take this behaviour into account, as ignoring it is unconservative in the serviceability and deformation estimates made in the design due to greater deflection as a result of slippage and stretching of the geosynthetic in the anchorage area.

Numerical simulations conducted by Villard et al. (2016) and

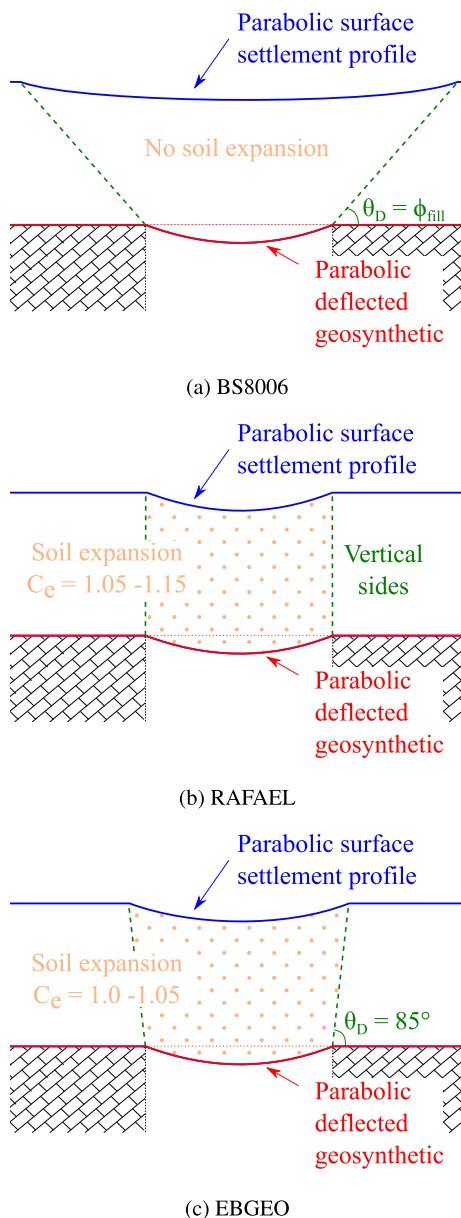


Fig. 3. Schematic representation of assumed soil and geosynthetic behaviour used in design methods for geosynthetic-reinforced soils above voids.

laboratory small-scale experiments by Pham et al. (2018) showed that the cavity opening process influences the shape of the load distribution acting on the geosynthetic. The load distribution was described as approximately conical for a progressive cavity diameter opening process, and an inverted parabola for the trapdoor process.

In summary, the primary design methods in use all assume a uniformly distributed vertical stress on the geosynthetic and corresponding parabolic deflection profile. This has been validated in some tests,

however, further numerical and experimental research conducted suggests that due to shearing in the soil, the true stress distribution is potentially more closely approximated by an inverse-triangular distribution. If the true distribution is inverse-triangular, then, for the same applied average stress (as calculated from soil arching), the current design procedures over-predict strains and deflections and would result in over-design of the required geosynthetic stiffness.

### 2.3.2. Soil surface settlement

The current design guidelines all consider the soil surface to follow a parabolic profile matching that of the geosynthetic. A comparison of the soil surface settlement profiles from the numerical simulations conducted by Potts et al. (2008) to the RAFAEL and BS8006 design guidelines showed that neither method provided an accurate prediction of the observed behaviour. The BS8006 settlement profile was much wider and smoother than the numerical results, which is unconservative in serviceability predictions where differential settlement is critical as the slopes of the Gaussian distribution would be steeper than a parabolic profile. Potts et al. (2008) showed that the use of a Gaussian distribution provided an excellent match to both the numerical results and a small-scale laboratory test conducted. Observation of the displacement vectors showed that the deformation in the fill is almost purely vertical, and limited largely to the area directly above the void. The consideration of the soil surface distribution as a Gaussian function was also used by Pham et al. (2018).

In related literature regarding trapdoor studies for soil arching without reinforcement, Costa et al. (2009) measured the surface settlement profile above a rectangular trapdoor overlain by both loose and dense sands, and showed that this matched a Gaussian distribution. This had been suggested earlier by similar tests by Evans (1983). This profile is consistent with the well characterised experimental work above tunnels (Peck, 1969; Mair, 2008). In the current design case, it would also be expected that a more appropriate assumption would be that the settlement profile follows a Gaussian distribution.

### 2.3.3. Shape of zone of subsidence

The failure zone shape in existing design methods varies from a cylinder/prism to a wide funnel based on the internal angle of friction (see Fig. 3). The tests conducted by Blivet et al. (2002) (which informed both the RAFAEL and EBGEO methods) showed that when failure of the soil body occurred, this was confined to a cylindrical zone above the cavity. The use of a failure model with vertical shear surfaces extending from the edge of the void was therefore proposed. No experimental validation of the wide funnel used by BS8006 has been made.

Pham et al. (2018) conducted an extensive series of laboratory tests (1 g) using a circular void, three soils types, two geosynthetics, and three  $H/D$  ratios (0.5, 1.0, 1.5) to investigate geosynthetic-reinforced soils above cavities. It was reported that the shape of the collapsed soil for the majority of tests resulted in a cylindrical failure zone; for very low  $H/D$  ratios, the formation of a narrow funnel was observed. The cylindrical failure zone was also reported in the analysis of full scale tests by Huckert et al. (2016) ( $H/D = 0.4, 0.8, 1.33$ ). This suggests that the failure models adopted by RAFAEL and EBGEO would be most appropriate in the design of geosynthetic-reinforced soils above voids.

From the literature, it would be expected that the settlement trough is likely to be wider than the void width, but much narrower than the funnel from the BS8006 prediction. These results are however limited to low  $H/B$  or  $H/D$  ratios and primarily circular voids; the implication

of extending these assumptions beyond the range of geometries tested has not been validated. Accurate estimate of the failure zone is required as if the predicted surface trough is too wide, this may be unconservative in the implications of degree of differential settlement; conversely, if it is too narrow, structures outside the predicted zone of influence that would be expected to be safe may be impacted by differential settlement.

#### 2.3.4. Soil expansion

Expansion in the soil is taken into consideration in some methods and not others, and is applied uniformly to the entire deforming soil body using a coefficient of expansion,  $C_e$ . The recommended values in the design codes were based on experimental results using settlements recorded above at the centre of the void and at the geosynthetic, and assuming parabolic deflection profiles for both surfaces.

As highlighted by Huckert et al. (2016), expansion in the soil above a void is unlikely to be a global phenomenon in the deformed soil, and there is no suitable methodology to determine the appropriate design value. Pham et al. (2018) measured the expansion coefficient for a range of soil densities using a Gaussian soil surface distribution and found that an increasing density results in a larger coefficient of expansion, which can be explained by the soils dilatancy. However, despite these observations and improved understanding of the mechanisms involved, there is still no method to accurately estimate the coefficient of expansion based on soil properties.

Consensus in the literature shows that even if the failure mechanism is a vertical column, the soil surface settlement is less than the geosynthetic settlement due to shearing in the fill which induces dilation and expansion. The assumption followed by BS8006 of ignoring soil expansion is thus not considered appropriate. However, an accurate estimation of this soil expansion and reduction in settlement remains elusive.

#### 2.4. Research objectives

It is important to ensure that the geosynthetic deflection and movement, shape of the subsidence zone, surface settlement profile, and the expansion behaviour are well understood to ensure that the design procedure for geosynthetic-reinforced soils above voids allows an accurate prediction of performance. Existing design guidelines vary widely in some areas, and are largely based on recommendations from a small number of tests with circular voids and shallow  $H/D$  ratios. These observations can therefore not readily be applied to thicker fills, or infinitely long voids. Further research has helped to address some of these uncertainties, but a complete understanding of the geosynthetic and soil deformation behaviour does not exist. No related centrifuge tests have been conducted.

The research presented in this paper aims to address these uncertainties through an experimental investigation into the soil and geosynthetic deformation mechanisms in a geotechnical centrifuge. This provides validation of the behaviour at an appropriate stress level, with visual observations and controlled boundary conditions allowing detailed measurements and analysis to be conducted.

### 3. Methodology

Centrifuge tests were conducted to investigate the behaviour of geosynthetic-reinforced soils above voids, using the lowering of a trapdoor between two stable abutments to simulate the void formation.

Centrifuge modelling provides an accurate replica of the stresses and strains of the expected field behaviour of the problem through the application of an increased gravity field. The ability to carefully control the model properties and boundary conditions, and record detailed measurements allows a thorough investigation into the soil and geosynthetic deformation mechanisms. The tests were conducted in the 10 m balanced beam geotechnical centrifuge at the Schofield Centre at the University of Cambridge (Schofield, 1980) at an acceleration of  $N = 40$  g. Full details are provided in da Silva (2017).

#### 3.1. Centrifuge package

A rigid, rectangular centrifuge model box built of an aluminium U-frame, steel back plate, and a steel framed Perspex window was used for the testing. A plane-strain model with the inclusion of a transparent boundary was chosen for the ability to capture high quality images of the deformation throughout the void formation process, and to use these to obtain accurate measurements of the soil and geosynthetic displacements using Particle Image Velocimetry (PIV) (Stanier et al., 2015).

The void was simulated by means of a 50 mm wide rectangular trapdoor (equivalent to a 2 m wide void) which was lowered between two rigid abutments. Sand was glued to the aluminium abutments to simulate a rough interface. The trapdoor displacement was controlled by a connecting the hydraulic cylinder below the trapdoor to an external cylinder with a linear actuator attached to the piston; raising the piston of the external cylinder caused the trapdoor to lower in a controlled manner. More details about the test set-up and trapdoor mechanism can be found in da Silva et al. (2016). An annotated photograph of the centrifuge package with the trapdoor is shown in Fig. 4.

#### 3.2. Granular soil

Dry Hostun sand (HN31), a fine grained siliceous sand from France, was used for the granular material. A mix of approximately 5% dyed blue sand was included to create more contrast allowing better tracking of strains and deformations by the PIV analysis.

The soil has an average particle size,  $d_{50}$ , of 0.356 mm; using the trapdoor width as the critical model dimension,  $B/d_{50} \approx 140$ , and particle size effects are therefore not expected to influence the observed soil behaviour (Iglesia et al., 2011). The sand model was prepared at a minimum relative density of 90% by using air pluviation in the automatic sand pourer as described by Zhao et al. (2006); this creates a consistent and uniform relative density of the soil. The measured shear strength from shearbox tests are shown in Table 2.

#### 3.3. Model geosynthetic

The selection of an appropriate model geosynthetic was based on scaling of the tensile strength-strain behaviour and interface compatibility as presented by Springman et al. (1992) and Viswanadham and König (2004). In the behaviour of geosynthetic-reinforced soils above voids, the dominant geosynthetic property influencing the behaviour is the material *stiffness*. The scaling laws required that the stiffness is reduced by a factor of  $N$  from the prototype (full-scale) to the model material.

The geosynthetic reinforcement requires a high stiffness and low-creep to limit the deflection in both the short and long-term Jones and Cooper (2005). Detailed evaluation of the impact of geosynthetic



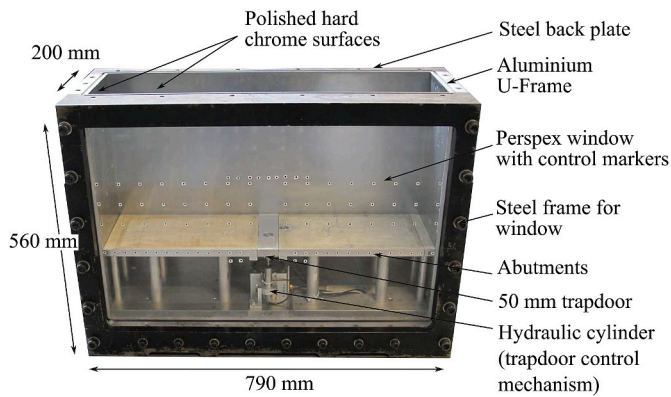


Fig. 4. Plane strain centrifuge package with trapdoor to simulate voids and Perspex window for image capture of soil displacements.

Table 2  
Friction and dilatancy angles from shearbox tests.

Normal stress $\sigma_n$ (kPa)	Relative density RD (%)	Peak strength $\varphi_p$ (°)	Critical strength $\varphi_c$ (°)	Peak dilation $\nu$ (°)
20	87.27	52.13	35.79	16.35
50	87.45	47.66	36.12	11.54
100	89.55	46.36	34.13	12.22

stiffness on the maximum geosynthetic deflection using the formulae presented in Table 1 showed that for small voids with low applied loads, increasing the stiffness of the geosynthetic beyond 2000 kN/m has limited additional benefit (da Silva, 2017).

A review of commercially available geosynthetic-reinforcements was conducted, and it was found that a target prototype stiffness of 1000 kN/m (model stiffness,  $J_m = 25$  kN/m) would provide a realistic approximation of materials commonly available for use in full-scale applications. It was also expected that a material of this stiffness would allow sufficient deformation to take place that could be visually monitored.

Preliminary tensile tests were conducted on a variety of model materials used by previous researchers, such as curtaining, nets, meshes, and bandage materials to identify a suitable model material. Two model geosynthetics were chosen for the centrifuge test series based on the manageability of the material and repeatability of the measured stiffness: a woven polyester pollen mesh and a curtain fabric. Photographs of these two materials are shown in Fig. 5; the aperture sizes and material thicknesses are indicated.

Pre-straining the mesh to 2.5 kN/m and curtain to 1 kN/m, and then unloading and reloading gave a repeatable, near-linear stress-strain response in the expected deformation range of 5% strain. Five loading and unloading cycles were applied to the model geosynthetic; the average of the final three cycles was used to determine the secant stiffness, and the results are shown in Table 3. The equivalent prototype stiffness of approximately 1124 kN/m and 811 kN/m for the mesh and curtain respectively match the target stiffness well, and allow a comparison on the effect of geosynthetic stiffness on the soil and geosynthetic deformation behaviour.

The geosynthetic interaction with the soil also needs to be

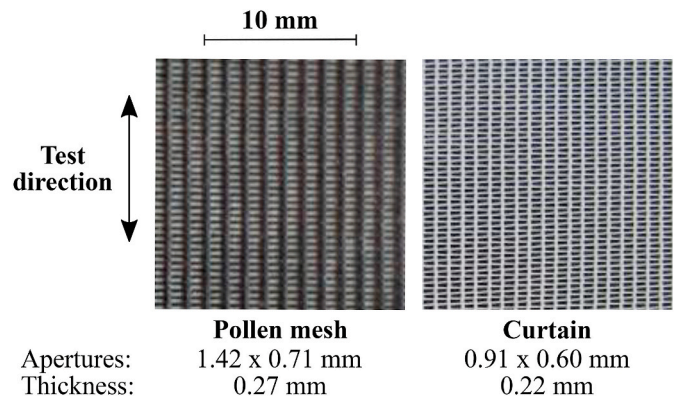


Fig. 5. Model geosynthetic materials.

Table 3  
Model geosynthetic properties.

Property	Units	Mesh	Curtain
2% secant stiffness	kN/m	28.11	20.27
5% secant stiffness	kN/m	26.46	20.18

considered. To ensure retention of the soil above the geosynthetic, soil-sheet behaviour needs to be replicated (soil particles are trapped in the apertures). Springman et al. (1992) show that for this to occur, the ratio of the geogrid aperture to the average particle size should be:  $s/d_{50} < 5$ . As dimensions scale linearly in the centrifuge (Taylor, 1995), a maximum aperture size of 1.78 mm is thus required with the Hostun sand ( $5 \cdot d_{50}$ ). The aperture dimensions of the model geosynthetics shown in Fig. 5 show that this criterion is met.

### 3.4. Test procedure

Three ratios of the soil height to void width,  $H/B = 1, 2$  and  $3$ , were tested with each geosynthetic (i.e. soil depths of 50, 100 and 150 mm respectively). These were selected as these are the boundaries indicated in EBGeo between different modes of behaviour, and would allow comparison of the deformation mechanism between thin and thick fills. A schematic representation of the test series reported in this paper is shown in Table 4.

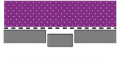





## 4. Results

### 4.1. Soil deformation

Particle image velocimetry (PIV), as described by Stanier et al. (2015), was used to observe the soil displacement, shear strains, and volumetric strains. The end of the test was determined as the point at which the PIV analysis between two successive images showed no observable differences in incremental displacement or strain. Photographs taken with the geosynthetic completely spanning the void are shown in Fig. 6 for the tests with the mesh-reinforcement.

The photographs show that for low  $H/B$  ratios, some deformation at the soil surface is visible, whereas for higher ratios this is not possible. A smooth settlement profile is evident from the horizontal blue lines and shows no sharp kinks or interference from shear bands.

**Table 4**  
Schematic configurations of the test layouts.

$H/B = 1$	$H/B = 2$	$H/B = 3$
 RNF-M-1	 RNF-M-2	 RNF-M-3
 RNF-C-1	 RNF-C-2	 RNF-C-3

The displacements and strains determined from the PIV are presented in the following sections. These results will be used in the identification of the deformation mechanisms in the further analysis of the results.

4.1.1. Displacement

The final soil displacements for the mesh-reinforcement are shown in Fig. 7. These results show that the deformation is localised to the zone above the void, with a slight funnel-shaped expansion towards the soil surface. A similar magnitude and extent of displacement is observed within each series (curtain-reinforcement results not shown), particularly between  $H/B = 2$  and 3.

In both test series, the highest deformation throughout the soil is observed where  $H/B = 1$ , as can be seen by the brighter colour of the shaded profile in the zone above the void. This is contrary to what may

be expected: typical arching calculations used for example in EBGeo and RAFAEL calculate that deeper fills apply greater stresses to the deflected geosynthetic. Thus it would be expected that the deeper fills (greater  $H/B$  ratios) deform more than shallower fills. An alternate understanding is that the load in the shallow test is higher than the deeper soils, as the benefit from the reduction due to arching is not as well established. Additionally, the lower confining stress on the geosynthetic in the anchorage area may be resulting in more pull-out of the geosynthetic from the abutment into the void, which would result in higher displacement of the geosynthetic and thus greater observed deformations. These assumptions will be confirmed with the analysis of additional results.

Superimposed displacement contours for each test series are plotted in Fig. 8a and b. The tests with the mesh-reinforcement have lower displacements directly above the void than those with the curtain-

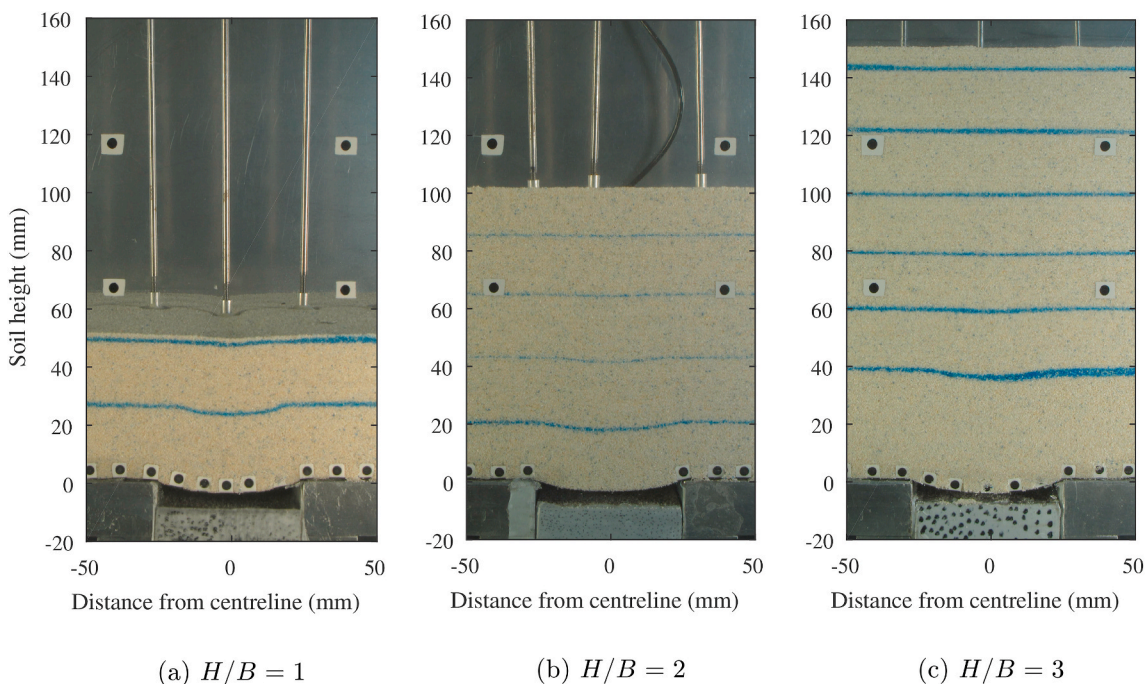


Fig. 6. Soil deformation photographs at the end of the test showing geosynthetic spanning over the void; images shown for mesh-reinforcement.

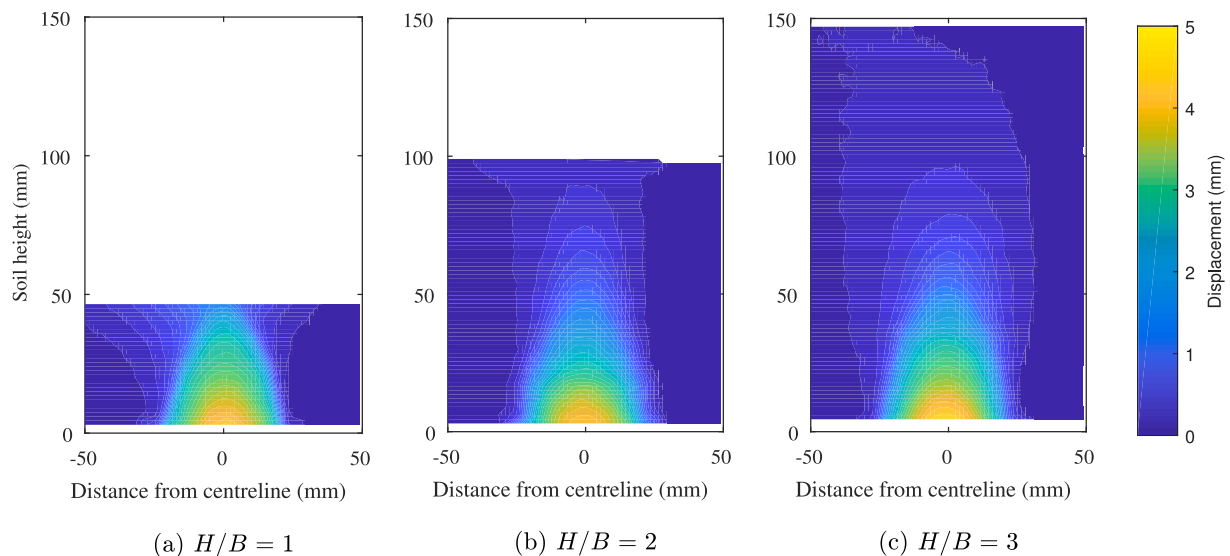


Fig. 7. Total displacements for mesh-reinforcement.

reinforcement. This is as expected as the mesh is stiffer than the curtain. The size and shape of the displacement contours is approximately equal in each series, indicating the formation of a unique soil deformation mechanism for each reinforcement. This deviates where the soil contours approach the soil surface, evident at  $h = 50$  mm for the  $H/B = 1$  tests.

A direct comparison between the two reinforcements using  $H/B = 3$  is shown in Fig. 8c, and it can be seen that the size and shape of the small-displacement contours ( $\leq 1.5$  mm) are approximately equal. This implies that the overall volume of soil engaged when the geosynthetic deflects above the void is the same, with different volumetric expansion within this total volume.

#### 4.1.2. Shear strain

The final maximum shear strains are plotted in Fig. 9; in both test series, the highest shear strains and clearest formation of shear bands (shear strain localisations) are observed in the tests with  $H/B = 1$ . Due to the distributed displacement, well defined shear bands which would separate near-rigid zones of soil movement were not observed. In addition, the sheared zone appears to be curvilinear. This is in contrast to the clear formation of linear shear bands forming a triangular deformation mechanism reported by da Silva Burke and Elshafie (2020a) for tests conducted with the same setup, but without reinforcement.

#### 4.1.3. Volumetric strain

The volumetric soil strains are plotted in Fig. 10; negative volumetric strain (blue) indicates soil dilation (i.e. expansion). This expansion is highly localised to a region above the void and within the boundary of the previously observed shear bands from Fig. 9; no planes of separation are observed in the soil.

In the tests with  $H/B = 2$  and 3, the volumetric strain appears to be approximately uniform across the zone of deformed soil. The average volumetric strain in the curtain-reinforcement tests appeared to be slightly higher than those in the mesh-reinforcement tests, although the size of the deformed zone is similar. This is expected from the observations made from the displacement contours in Fig. 8.

As per the maximum shear strains, the tests with  $H/B = 1$  had the highest observed volumetric strains. The low confining pressure results in higher dilation in the soil and therefore greater expansion. In these two tests, the volumetric strain is predominantly concentrated in the shear band zones observed in the maximum shear strains and not distributed uniformly through the soil as was observed when  $H/B = 2$  and 3.

## 4.2. Geosynthetic deflection

### 4.2.1. Maximum deflection

The maximum geosynthetic deflection,  $d$ , was determined from the PIV conducted on the soil in contact with the geosynthetic above the void; the results are shown in Table 5. The deflection was approximately equal for each type of geosynthetic-reinforcement used.

### 4.2.2. Deflected geosynthetic profile

The deflected geosynthetic profile was determined from a photograph after the end of the test where the geosynthetic was clearly spanning the void. The profile was determined based on the light intensity in the image, using a threshold intensity value to specify the soil/void boundary. The final smoothed profile was determined after filtering to remove the noise, and was converted from pixels to millimetres using the PIV photogrammetric calibration. For test RNF-C-1 where soil falling in front of the spanning geosynthetic obscured a clear



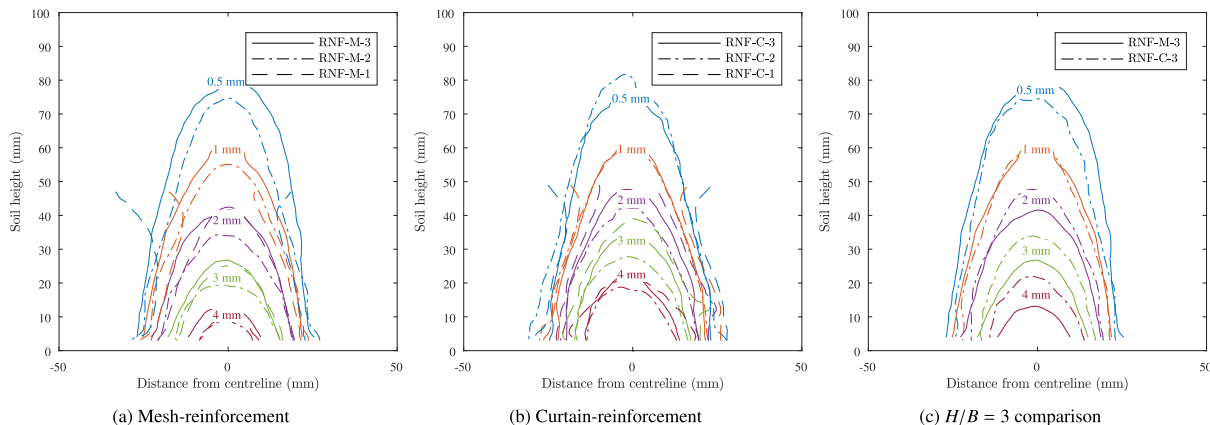


Fig. 8. Superimposed displacement contours.

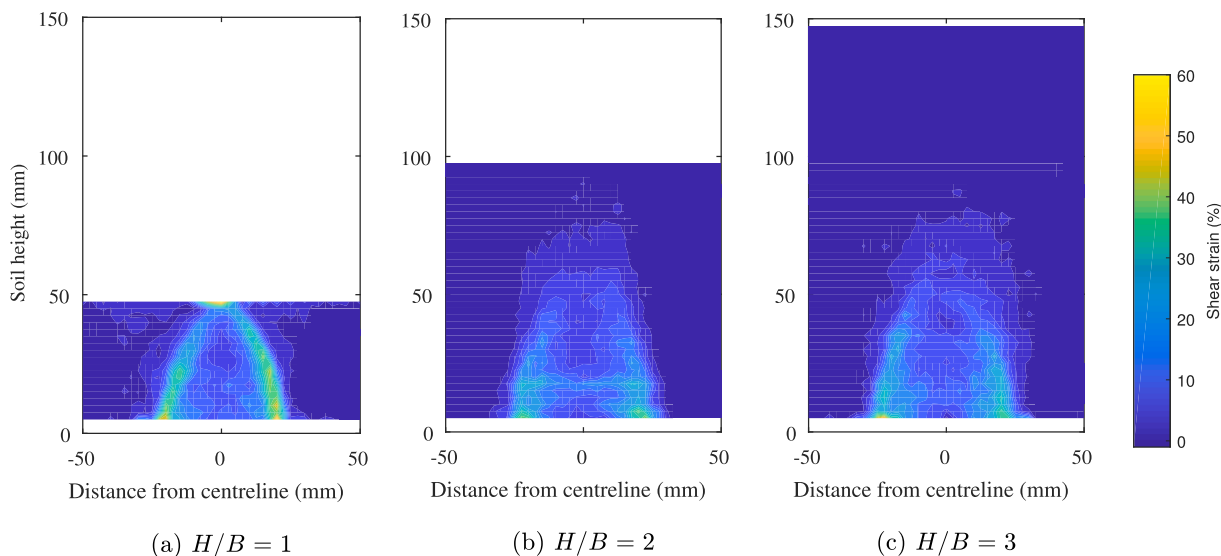


Fig. 9. Maximum shear strains; images shown for mesh-reinforcement.

view, the profile was manually determined by comparing the stable regions where soil was not moving; this results in a larger error in the determination of the final deflected shape than the automatic method. The deflected geosynthetic profiles are shown in Fig. 11; these have been normalised by  $d$  to allow a comparison of the shapes between the tests.

The deflection profiles were compared to a parabolic, cubic, and cubic-quadratic shape (Table 1) fitted through  $d$  to identify which stress distribution and resulting deflection profile most accurately matched the observed behaviour. These shapes are included in Fig. 11 for comparison to the observed profiles. The circular profile was not used due to its similarity to the parabolic profile at low deflections (see Fig. 2).

The observed profile fits primarily in-between the cubic (inverse-triangular stress distribution) and parabolic profile (uniform stress distribution); the stress distribution on the geosynthetic above the void could therefore be assumed to be in-between a uniform and inverse-triangular shape, either a superposition of the two, or potentially an inverted parabolic as suggested by Villard et al. (2016) and Pham et al. (2018). The tests with the mesh-reinforcement, which had lower deflections, generally showed a closer fit to the cubic profile; the curtain-reinforcement, which had higher deflections, showed a closer fit to the parabolic profile. This is similar to the conclusion from Huckert et al. (2014) where the larger sinkhole which would have greater deflections has a uniform distribution, and the smaller sinkhole with smaller deflections has an inverse-triangular stress distribution. The results were

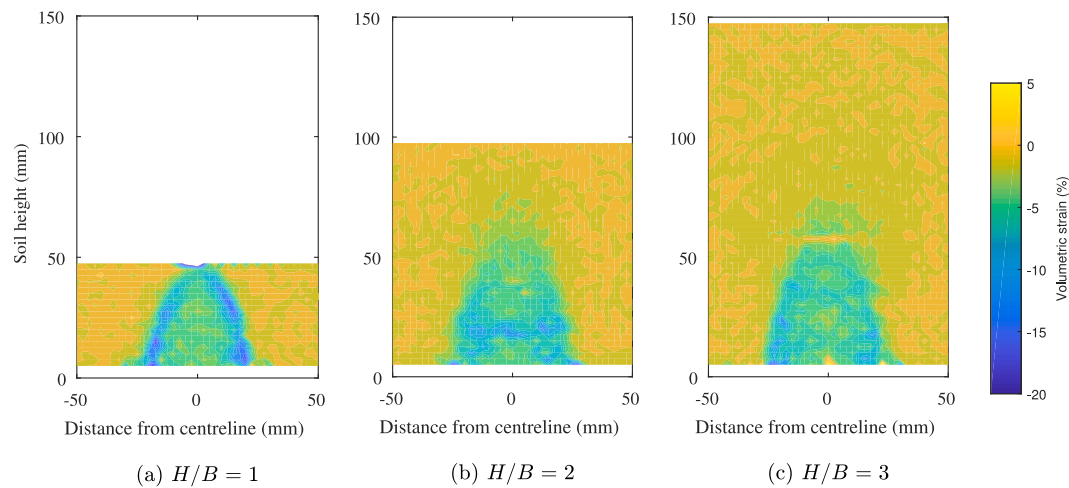


Fig. 10. Volumetric strains (negative: dilation; positive: contraction); images shown for mesh-reinforcement.

not considered consistent enough for the proposal of a unique deflection profile and inferred stress distribution that exactly matched these centrifuge test results. Differences between the clear inverse-triangular distribution shown in van Eekelen and Bezuijen (2012) and the superimposed uniform and inverse-triangular suggested in the current results are potentially due to differences in experimental setup, notably individual piles versus a trapdoor. Further research is required to investigate this in more detail.

The existing design methods calculate the strain in the geosynthetic from a calculated applied stress; for the same average stress, the parabolic profile results in higher deflections and strains than the cubic profile (see Fig. 2). Thus, based on the results presented thus far and the uncertainty in giving a clear indication of the exact deflected profile, the conservative approach for a recommended design procedure would be to assume that the geosynthetic deflection profile is parabolic in shape. Because the actual deflection profile is in-between the cubic and parabolic profiles, this is not significantly overconservative. As the load distribution is related to shearing in the soil and soil arching, further consideration to the load-distribution and appropriate membrane effect calculations is given in da Silva Burke and Elshafie (2020b).

#### 4.2.3. Movement in the anchorage area

Markers were glued onto the geosynthetic to track the movement in the anchorage area; these can be seen in Fig. 6. The markers were tracked using PIV; the final horizontal movements are plotted in

Table 5  
Maximum geosynthetic deflection.

Test	Deflection, model scale (mm)	
	<i>d</i>	<i>d<sub>ave</sub></i>
RNF-M-1	4.87	4.71
RNF-M-2	4.36	
RNF-M-3	4.91	
RNF-C-1	5.73	5.54
RNF-C-2	5.27	
RNF-C-3	5.63	

Fig. 12.

The results showed that there was movement of the geosynthetic in the anchorage area, with a maximum value of ± 0.5 mm for the mesh-reinforcement and ± 1.0 mm for the curtain-reinforcement at the trapdoor edges. The movement generally decreased with increasing height of the soil; this is due to the increased vertical stress which secures the geosynthetic in position in the anchorage area and confirms the expectations made in the observations of the soil displacements (see Section 4.1.1). The movement was confined to a region approximately half the void width outside the trapdoor edges and is expected to be due to the combination of taking up slack in the laid-out geosynthetic, and the mobilisation of the geosynthetics strength as it stretches above the void.

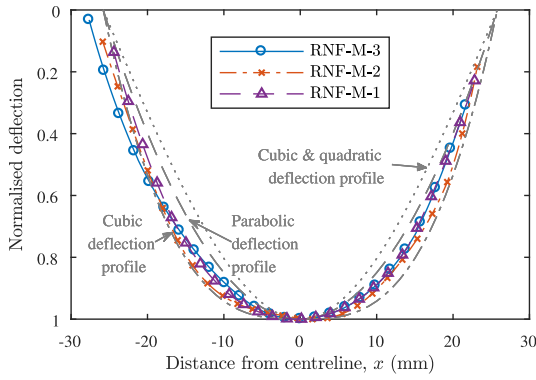
## 5. Analysis and discussion

### 5.1. Summary of deformation mechanisms

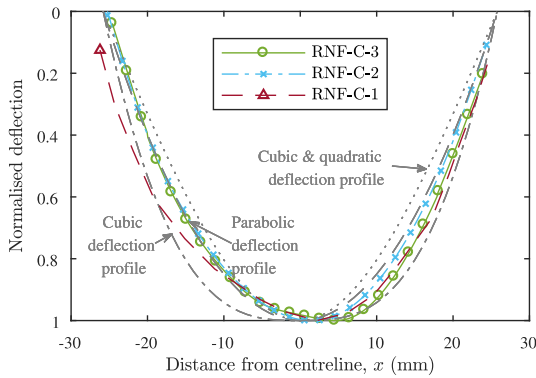
The PIV displacement and strain results showed the development of a single deformation mechanism in the soil. The energy dissipation occurred primarily via volumetric strain and expansion of the soil above the void to take up the space created by the deflecting geosynthetic.

The PIV results showed that comparing the displacements and strains between all the reinforced tests, an approximately constant volume of soil appeared to be engaged in the energy dissipation. A parabola bound by the angle of dilation,  $\nu$ , to the vertical at the trapdoor edge provides an excellent match for the observed location of shear bands and extent of the volumetric strain. This result is shown in Fig. 13 using  $\nu$  from Table 2 for the relevant stress level. This parabola was also found to coincide approximately with the 1 mm displacement contour (see Fig. 8).

The dependency of the shape and size of the shear and volumetric strains on the angle of dilation explains why in both series of tests, the behaviour of the tests when  $H/B = 3$  and 2 is the same, but deviates when  $H/B = 1$ . For both  $H/B = 3$  and 2 ( $\sigma_v = 96,64$  kPa), the peak angle of dilation is  $12^\circ$ ; thus the size of the parabola and general soil behaviour is expected to be the same. For  $H/B = 1$  ( $\sigma_v = 32$  kPa),  $\nu = 16^\circ$



(a) Mesh-reinforcement



(b) Curtain-reinforcement

Fig. 11. Observed geosynthetic deflection profiles with fitted shapes shown.

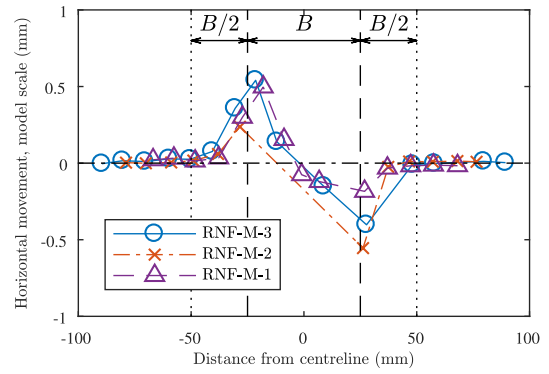
due to the lower confining stress, resulting in a narrower, more well-defined parabola. This provides a simple and convenient model for predicting the zone of the soil affected by expansion as the geosynthetic deflects over the void, which has not been done before.

### 5.2. Surface and sub-surface settlement profiles

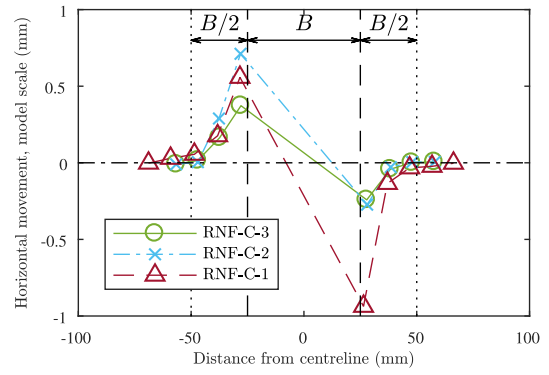
The final surface and sub-surface soil settlement profiles obtained from PIV analysis are shown in Fig. 14. The results showed that within each test series, similar settlement profiles are observed through the height of the soil, as would be expected from the contour comparisons in Fig. 8. Wide, shallow settlement profiles were evident at the surface of the deepest test, with narrower, deeper profiles observed nearer to the geosynthetic.

Standard Gaussian distributions of the form shown in Equation (1) were fitted to the observed profiles, where  $s_v(x)$  is the vertical settlement of the soil at distance  $x$  from the centreline,  $s_{max}$  the maximum vertical settlement, and  $i$  the horizontal distance measured from  $s_{max}$  to the inflection point of the curve.

$$s_v(x) = s_{max} e^{-0.5(x^2/i^2)} \quad (1)$$



(a) Mesh-reinforcement



(b) Curtain-reinforcement

Fig. 12. Observed horizontal displacements in the geosynthetic anchorage area.

A modified Gaussian distribution as developed by Vorster et al. (2005) shown in Equation (2) was also fitted to the settlement curves; this allows an additional degree of freedom,  $n$ , and includes a shape factor,  $\alpha$ , which is used to alter the vertical location of the point of inflection and has the effect of steepening the curve and controlling the trough width. The modified curve is equivalent to the standard curve when  $\alpha = 0.5$  ( $n = 1$ ).

$$s_v(x) = \frac{n}{(n-1) + e^{\alpha x^2/i^2}} s_{max} \quad (2)$$

$$n = e^{\alpha \frac{2\alpha-1}{2\alpha+1}} + 1$$

An example of the fitted Gaussian and modified Gaussian curves for test RNF-C-3 is shown in Fig. 15. As expected due to the ability to modify the shape, the modified profile showed an overall better match. This is most notable closer to the geosynthetic, with less difference at the surface. The use of the standard Gaussian distribution requires one variable less to be estimated, and thus, although this distribution has a slightly poorer fit to the data, it may be preferable in routine use, especially for greater soil heights where the difference between the standard and modified Gaussian distribution is marginal.

The fitted inflection point from the standard Gaussian curves and

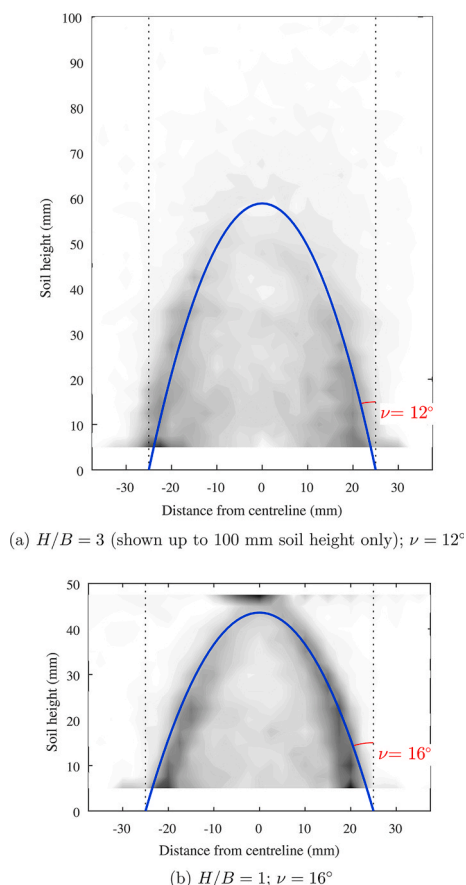


Fig. 13. Parabolic fit to observed shear strain profiles.

the normalised inflection point ( $i/h$ ), also referred to as the trough width parameter in investigations in tunnels,  $K$  (Mair and Taylor, 1997), are plotted in Fig. 16 for all the tests. The results show a remarkably similar match and are virtually indistinguishable, except for test RNF-M-3. Due to the similarity of the results, this is expected to be an anomaly, although further verification is required.

Above  $h/B = 1$ , a constant value of  $i/h = 0.2$  is observed. Mair and Taylor (1997) recommend a value of  $K = 0.25 - 0.45$  at the surface for tunnels in sands and gravels; they observe an increase in  $K$  with depth, similar to what is observed below  $h/B = 1$  in Fig. 16. The lower equivalent  $K$ -value is consistent with the formation of a narrower mechanism where the deformation is limited by the geosynthetic deflection. An investigation by Marshall et al. (2012) into surface and sub-surface settlements in sands also showed a tendency for a constant value of  $K$  further away from the tunnel.

### 5.3. Shape of zone of subsidence

The width of the settlement trough,  $w$ , is calculated from the fitted  $i$  using Equation (3) (Costa et al., 2009). A constant inflection implies a constant trough width, and a constant normalised inflection implies the formation of a funnel-shaped zone of subsidence.

$$w = 2i\sqrt{2\pi} \tag{3}$$

The variation of trough width through the soil height is plotted in Fig. 17 by assuming that the calculated total width from Equation (3) occurs symmetrically across the centre of the void. This thus shows the shape of the zone of subsidence. The tests all behaved consistently with each other, with the exception of RNF-M-3 which was observed to have much wider settlement troughs above the transition point.

The shape can be summarised as being vertical from the base until the transition height where  $h/B = 1$ . The observed trough width is slightly wider than the trapdoor width; the average measured width is  $\approx 1.2B$ . This agrees with the failure mechanisms used by EBGeo and RAFAEL and matches the soil height ratios used in the tests that formed the basis of these codes. Above this transition point the geosynthetic limits the formation of the prismatic failure zone and the zone of subsidence increases linearly with height towards the surface; this can be inferred from the constant normalised inflection ( $i/h$ ) in this zone. The observed angle of draw in the tests conducted was  $\theta_D = 60^\circ$ .

### 5.4. Soil expansion

The RAFAEL and EBGeo design methods use a coefficient of expansion,  $C_e$ , to estimate the soil settlement,  $s$ , as a function of the geosynthetic deflection. This is calculated by considering the volume variation in the zone of subsidence. To evaluate the validity of this soil expansion model,  $C_e$ , was calculated from the trough volumes of the measured soil settlement profiles assuming the formation of a vertical failure zone equal to the trapdoor width throughout the soil (Equation (4)). Above  $h/B = 1$  where the subsidence zone widens, this  $C_e$  will be an upper estimate as the actual initial volume will be bigger due to the funnel mechanism.

$$C_e = 1 + \frac{\Delta V}{V_i} = 1 + \frac{V_{GSY} - V_{soil}}{Bh} \tag{4}$$

Fig. 18 shows that the use of a single, uniform coefficient of expansion to describe the relationship between the soil settlement and the geosynthetic deflection is inappropriate.  $C_e$  is not a unique value for a certain type of soil: the soil type, density, and stress level are equivalent between the two series of tests, but the calculated  $C_e$  varies. The calculated value is largely within the recommended ranges of EBGeo (1.03 – 1.05) and RAFAEL (1.05 – 1.15), but varies with height and is not a unique number for a given geometry. This suggests that this is not a suitable model for predicting soil behaviour as a function of geosynthetic behaviour.

An alternative visualisation of the expansion through the soil is



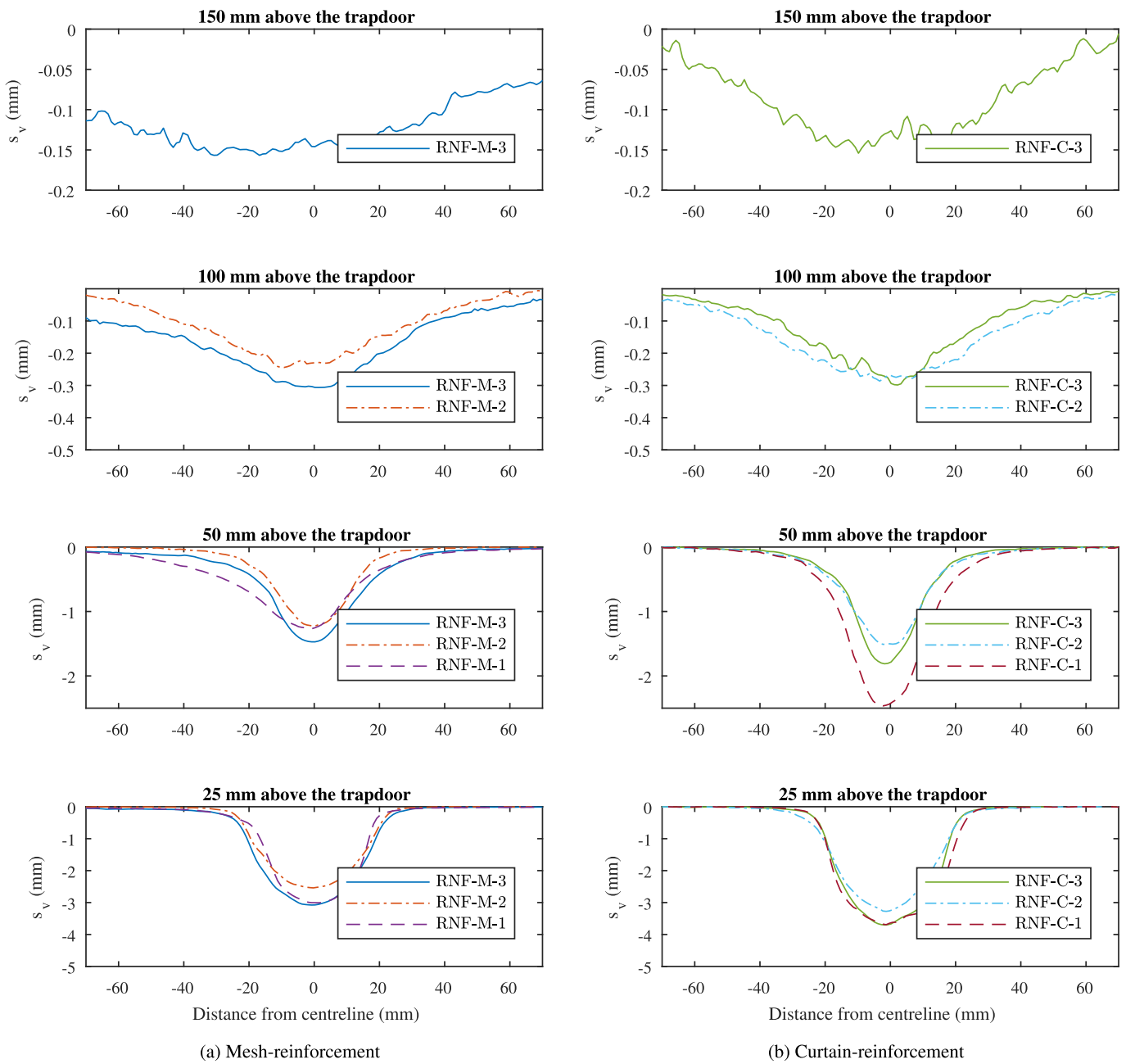


Fig. 14. Surface and sub-surface settlement profiles (curtain-reinforcement).

provided by plotting the maximum settlement to geosynthetic deflection ratio ( $s_{max}/d$ ) as a function of the height of soil above the trapdoor. Additionally, a plot of the ratio of the settlement trough volume to the volume of displaced soil at the geosynthetic level ( $V_{soil}/V_{GSY}$ ) with the soil height can be made. The results are plotted in Fig. 19.

The settlement ratio clearly shows that for the normalised settlement through the height of the soil, a single relationship can be used to describe the behaviour regardless of the geosynthetic deflection or total soil height. The volume ratio shows that the volume of the soil settlement trough tends to a constant value with increasing soil height. The

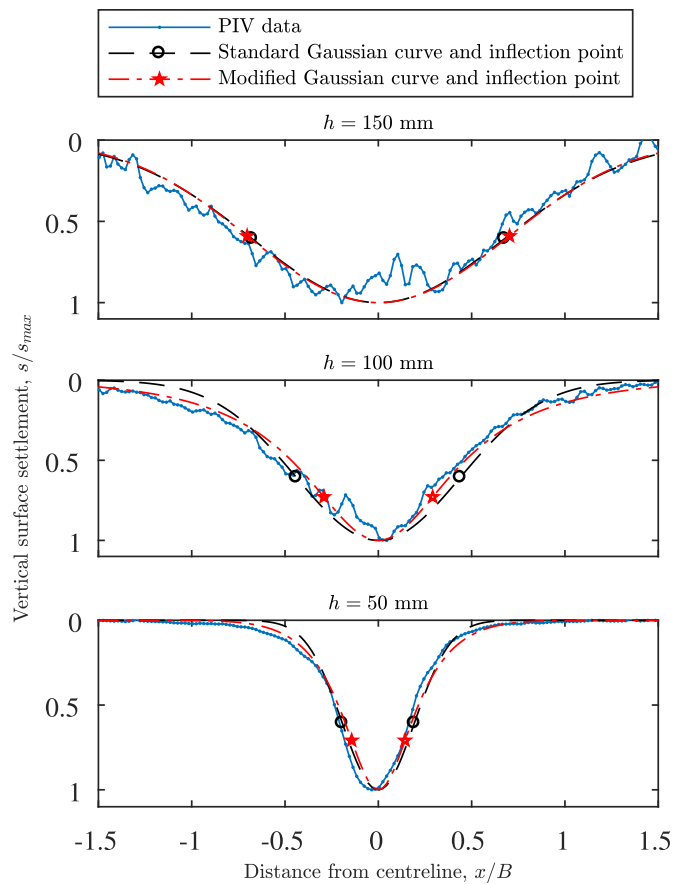


Fig. 15. Settlement curve fitting results: example shown for RNF-C-3.

settlement ratio still changes in this region as the trough width increases towards the surface. This confirms the observations made from the volumetric strains (Fig. 10) that the soil expansion is limited to a confined volume of soil above the void.

The height of the parabolic deformation mechanism identified in Fig. 13 has been indicated in Fig. 19b. This height appears to act as an inflection point between the region of soil where there is uniform expansion, and the region of soil where there is no more expansion with only the residual expansion as a result of the deformation lower in the soil body remaining. This is similar to the approach adopted in tunnelling in sands, where the volume loss at the surface is estimated as a function of the volume loss at the tunnel (Marshall et al., 2012).

A simple model of the soil expansion through the height of the soil would be to assume a constant expansion in the soil from  $V_{soil}/V_{GSY} = 1$  at the base, to a residual volume ratio of 0.1 at the height of the

parabola. For soil heights greater than this, the volume ratio will remain constant at this value as there is no further volumetric expansion outside of this zone. This model is plotted in Fig. 19b. In reality, there is a slight transition which means that this simplified model will slightly underestimate the volume loss in the soil in this transition zone. This model is based on tests all conducted at a single relative density; the validity of this model for a range of soil types and densities is subject to further research.

## 6. Recommendation

The observed soil and geosynthetic behaviour and analysis thereof can be used to make recommendations for modifications to the current procedures adopted in the design of geosynthetic-reinforced soils above voids. These suggestions are based on a small number of tests with a single soil type and density, and a limited range of  $H/B$  ratios and geosynthetic alternatives; the conclusions are thus not necessarily universally applicable, but provide a basis for exploring a more comprehensive understanding of soil and geosynthetic behaviour above voids.

A schematic representation of the observed soil and geosynthetic behaviour is shown in Fig. 20; this understanding can be used to make recommended improvements to the design procedures currently used. The fundamental basis remains the same, i.e. a maximum differential settlement at the soil surface is specified as the design criteria. Based on the assumed shape of the zone of subsidence, surface settlement profile, expansion in the soil, and deflected geosynthetic shape, the maximum geosynthetic deflection is calculated. This is combined with the calculated applied stress on the geosynthetic from arching theory to determine the minimum required stiffness of the geosynthetic; further discussion on soil arching in the context of reinforced soils over voids is given by da Silva Burke and Elshafie (2020b). As slippage of the geosynthetic is observed to occur, the modifications suggested by Briançon and Villard (2008) and Villard and Briançon (2008) need to be incorporated into the design. The primary difference is the use of a Gaussian distribution to define the soil settlement surface profile, and the assumption that the soil engaged in the expansion when the void forms is bound by a parabola with angles to the vertical equal to the dilation angle. Outside this area, the soil does not expand, and the volume of the soil settlement trough is related to the volume of the deflected geosynthetic by a residual value due to the movement of the parabolic boundary.

The recommended design procedure that follows the description of mechanisms from the reported tests in this paper is shown in Fig. 21. Further investigation is needed for characterisation of the width of the vertical failure zone, the height of the transition from the prism to the funnel, the angle of draw of the funnel and/or the normalised inflection point for the settlement curves, the fit of the parabolic deformation mechanism, and the residual expansion outside of this parabolic region in a wider range of soil types, densities and geosynthetic stiffnesses before conclusive statements of the wider applicability of this design procedure can be made.

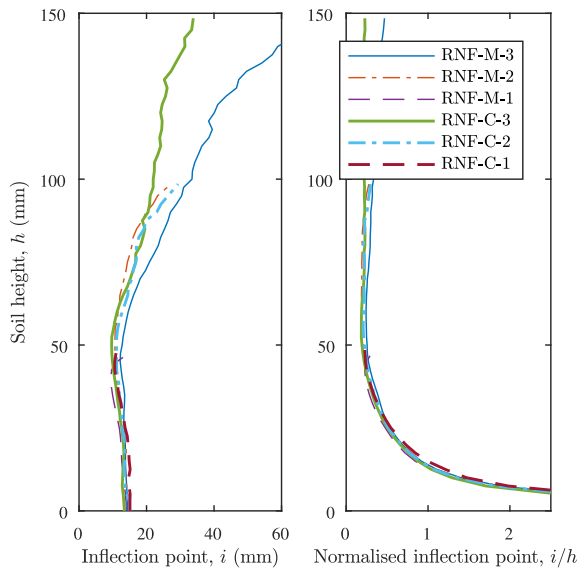


Fig. 16. Fitted inflection point and normalised inflection point for standard Gaussian settlement distributions.

7. Conclusion

Existing design methods for geosynthetic-reinforced soils above voids have large uncertainty and variations in the assumptions of the geosynthetic and soil behaviour which influences the appropriate design of these systems. Centrifuge tests were conducted to visually

observe the mechanisms of deformation in the soil body when a geosynthetic deflects into a void created by lowering a trapdoor. The interpretation of the results in terms of the four key assumptions made in the design procedure are summarised below.

- (i) Geosynthetic behaviour: The geosynthetic behaviour showed that a parabolic deflection profile, as would be created by a uniform vertical stress distribution, is a reasonable, albeit conservative, estimate of the true behaviour. This is in accordance with the adopted profile in all the design methods. The true profile is expected to lie between the parabolic and cubic profiles with a stress distribution which is non-uniform (greater at the edges); further investigation is required to more accurately characterise the deflected shape and load distribution. The centrifuge tests showed that there was stretching and displacement of the geosynthetic adjacent to the void. For low overburdens and critical infrastructure this effect must be considered using the procedure detailed by Villard and Briançon (2008).
- (ii) Soil surface settlement: The surface settlement profile is better described by a Gaussian distribution than the parabolic profile used by all the design methods. The Gaussian distribution has steeper sides than the parabolic profile, and for the same width and maximum settlement would result in more critical impacts on infrastructure.
- (iii) Shape of zone of subsidence: The shape of the zone of subsidence was a combination of a vertical and funnel-shaped failure mechanisms, and thus wider than assumed by EBGeo and RAFAEL, and far narrower than the BS8006 model. The vertical zone extended up to a height equivalent to the void width ( $h/B = 1$ ), with a width of  $1.2B$ . Above this level, a funnel with an angle of draw of  $60^\circ$  was observed.

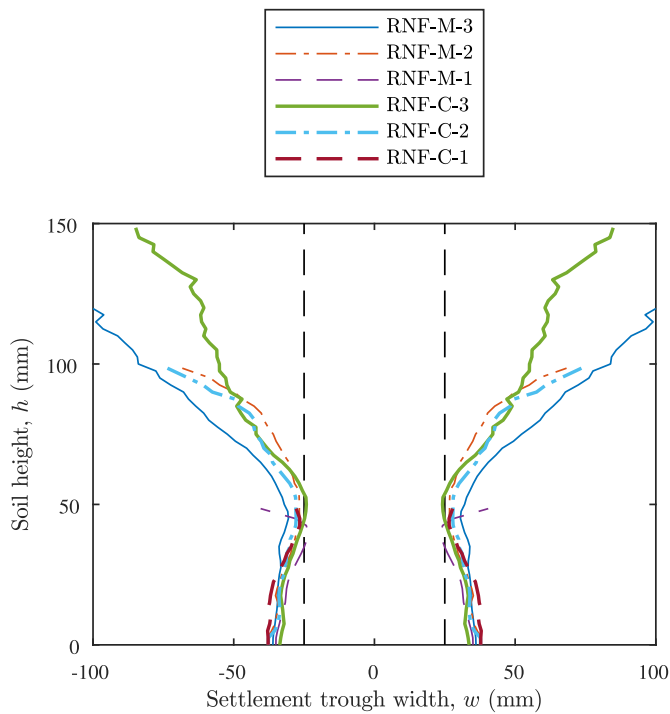


Fig. 17. Variation of calculated trough width with soil height.

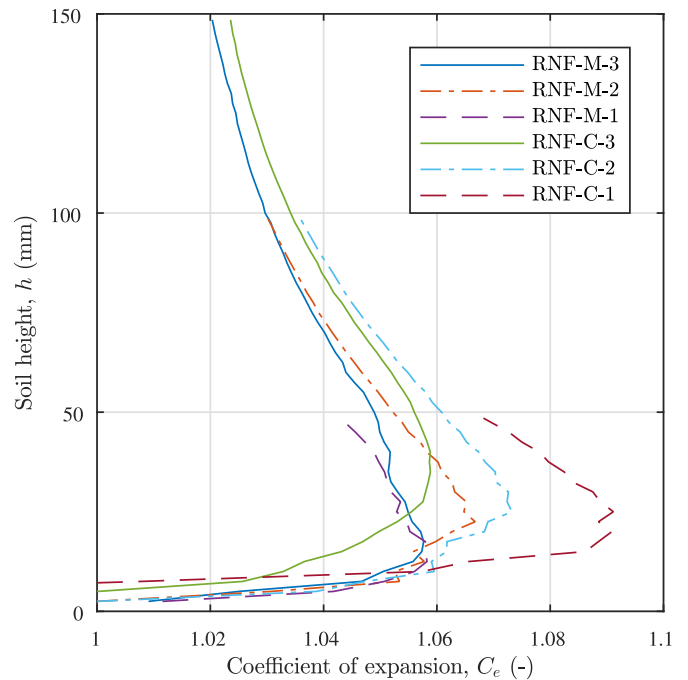
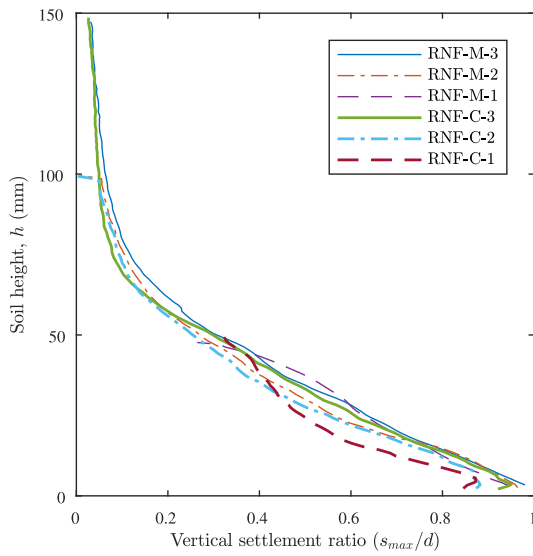
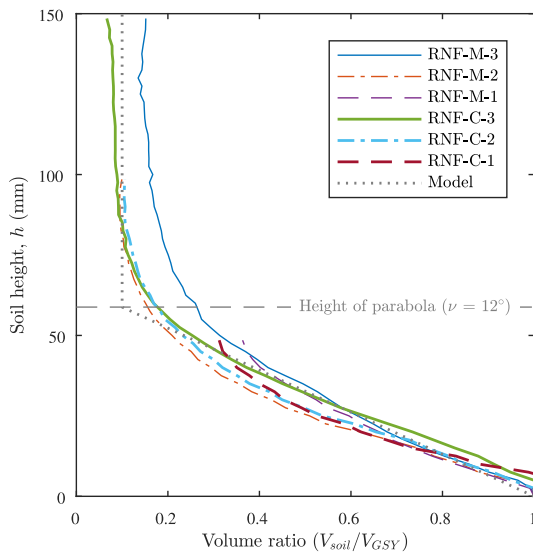


Fig. 18. Calculated coefficient of expansion,  $C_e$ , using the observed volume loss and assuming a vertical failure zone.



(a)



(b)

Fig. 19. Normalised settlement and volume ratio as a function of soil height.

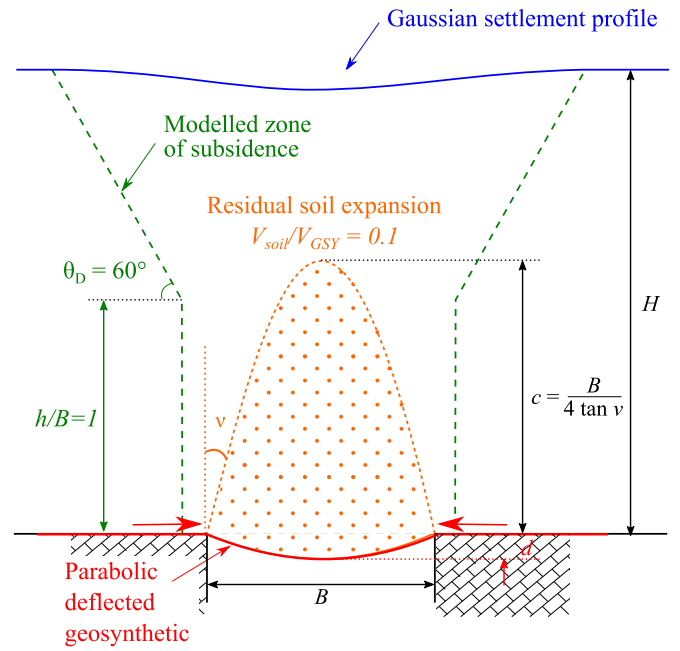


Fig. 20. Schematic representation of observed soil and geosynthetic behaviour in centrifuge tests.

(iv) Soil expansion: Soil expansion was observed in a localised region above the geosynthetic. A single, unique, coefficient of expansion as used by EBGeo and RAFAEL proved inadequate to describe the soil behaviour. The use of a model with a parabolic zone of expansion in the soil above the void, bound by the angle of dilation to the vertical at the void edges was accurately able to predict the extent and magnitude of expansion in the soil.

These observations confirmed some of the expected behaviour as highlighted in the limitations to the current design methodologies. A set of results has been provided which can inform further research and investigation into the most accurate designs and prediction of behaviour, allowing efficient designs based on thorough understanding of the soil and geosynthetic behaviour. These observations were based on a single void size, and soil type and density. More work is required using a variety of soils and void sizes to provide further validation. Whilst these limitations exist, the results provide a useful contribution



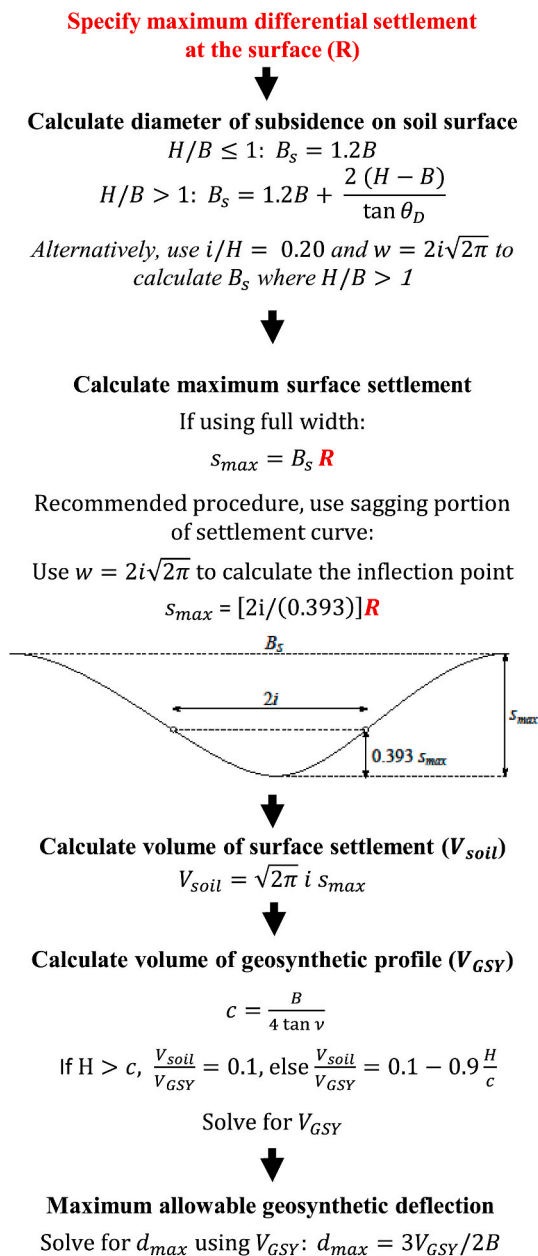


Fig. 21. Recommended design procedure following the description of mechanisms from the reported tests.

to the knowledge in the visualisation and description of the deformation mechanisms of reinforced-soils above voids.

### Acknowledgements

The centrifuge tests reported in this paper were conducted at the Schofield Centre at the University of Cambridge. Thanks are due to the technicians and staff for their assistance. The first author would like to acknowledge the Gates Cambridge Scholarship for financial support.

### List of symbols

$B$	Width of trapdoor, or width of infinitely long void (m)
$c$	Height of the parabolic deformation mechanism formed in the soil (m)
$C_e$	Coefficient of expansion
$D$	Diameter of circular void (m)
$d$	Geosynthetic deflection above void (m)
$d_{50}$	Average particle size (m)
$H$	Total soil height (m)
$h$	Soil height above base (m)
$i$	Distance from centreline to point of inflection on Gaussian distribution (m)
$J$	Geosynthetic stiffness (kN/m)
$K$	Trough width parameter
$N$	Gravitational acceleration factor of centrifuge
$n$	Additional degree of freedom in modified Gaussian distribution
$p$	Vertical stress at the base of a yielding soil (kPa)
$R^2$	Coefficient of determination to determine goodness of fit
$s_l$	Geogrid aperture size (m)
$E s_{max}$	Maximum soil settlement (m)
$s_v$	Vertical soil settlement (m)
$q$	Surcharge stress applied on the soil surface (kPa)
$T_0$	Horizontal tension in deflected geosynthetic (kN/m)
$V_{GSY}$	Volume of the deflected geosynthetic per metre width (m <sup>2</sup> )
$V_{soil}$	Volume of the soil settlement trough per metre width (m <sup>2</sup> )
$w$	Width of the settlement trough (m)
$x$	Distance from the centre of the deflected geosynthetic or soil settlement profile (m)
$\alpha$	Shape factor to modify slope and trough width in modified Gaussian distribution
$\varphi_c$	Critical angle of friction of the soil (°)
$\varphi_p$	Peak angle of friction (°)
$\rho$	Radius of curvature in circular deflected geosynthetic (m <sup>-1</sup> )
$\theta_D$	Angle of draw for funnel-shaped zone of subsidence (°)
$\nu$	Angle of dilation of the soil (°)

### References

- Bezuijen, A., van Eekelen, S.J.M., 2014. Basal reinforced piled embankments: validation of inverse triangular load distribution with an extended Terzaghi equation. In: Proceedings of the 10th International Conference on Geosynthetics. Berlin, Germany.
- Blivet, J., Gourc, J., Villard, P., Giraud, H., Khay, M., Morbois, A., 2002. Design method for geosynthetic as reinforcement for embankment subjected to localized subsidence. In: Proceedings of the 7th International Conference on Geosynthetics. Nice, France, pp. 341–344.
- Briançon, L., Nancey, A., Villard, P., 2005. Development of Geodetect: a new warning system for the survey of reinforced earth constructions. *Studia Geotechnica Mech.* 27 (1–2), 21–32.
- Briançon, L., Villard, P., 2008. Design of geosynthetic-reinforced platforms spanning localized sinkholes. *Geotext. Geomembranes* 26 (5), 416–428.
- BS8006, 2010. Code of Practice for Strengthened/reinforced Soils and Other Fills. British Standards Institution, London.
- Cooper, A.H., Calow, R., 1998. Avoiding gypsum geohazards: guidance for planning and construction. *Tech. Rep., Br. Geol. Surv., Tech. Rep. WC/98/5.*
- Costa, Y.D., Zornberg, J.G., Bueno, B.S., Costa, C.L., 2009. Failure mechanisms in sand over a deep active trapdoor. *J. Geotech. Geoenviron. Eng.* 135 (11), 1741–1753.
- da Silva, T.S., 2017. Centrifuge Modelling of the Behaviour of Geosynthetic-Reinforced Soils above Voids. Ph.D. thesis. University of Cambridge.
- da Silva, T.S., Elshafie, M.Z.E.B., 17 – 20 July 2018. Observed deformations in geosynthetic-reinforced granular soils subjected to voids. In: Proceedings of the 9th International Conference on Physical Modeling in Geotechnics (ICPMG 2018). London, United Kingdom. pp. 1169–1174.

- da Silva, T.S., Elshafie, M.Z.E.B., Madabhushi, G.S.P., 2016. Centrifuge modelling of arching in granular soils. In: Proceedings of the 3rd European Conference on Physical Modelling in Geotechnics. Nantes, France, pp. 301–306.
- da Silva Burke, T.S., Elshafie, M.Z.E.B., 2020a. Arching in Granular Soils: Experimental Observations of Deformation Mechanisms. *Geotechnique*. <https://doi.org/10.1680/jgeot.19.P.174>. (published online ahead of print 17 June).
- da Silva Burke, T.S., Elshafie, M.Z.E.B., 2020b. Geosynthetic-reinforced Soils above Voids: Experimental Observation and Prediction of Soil Arching. *Geotechnique*. <https://doi.org/10.1680/jgeot.19.P.175>. (published online ahead of print 17 June).
- EBGEO, 2010. Recommendations for Design and Analysis of Earth Structures Using Geosynthetic Reinforcements-EBGEO, second ed. Ernst & Sohn.
- Evans, C.H., 1983. An Examination of Arching in Granular Soils. Master's thesis. Massachusetts Institute of Technology.
- Galve, J.P., Gutiérrez, F., Guerrero, J., Alonso, J., Diego, I., 2012. Optimizing the application of geosynthetics to roads in sinkhole-prone areas on the basis of hazard models and cost-benefit analyses. *Geotext. Geomembranes* 34, 80–92.
- Gourc, J.P., Villard, P., 29–31 May 2000 2000. Reinforcement by membrane effect: application to embankments on soil liable to subsidence. In: In: Proceedings of the 2nd Asian Geosynthetics Conferen. Kuala Lumpur, Malaysia, pp. 55–72.
- Huckert, A., Briçon, L., Villard, P., Garcin, P., 2016. Load transfer mechanisms in geotextile-reinforced embankments overlying voids: experimental and analytical approaches. *Geotext. Geomembranes* 44 (3), 442–456.
- Huckert, A., Garcin, P., Villard, P., Briçon, L., Auray, G., 21 - 25 September 2014. Experimental and numerical approaches of the design of geotextile reinforced embankments prone to sinkholes. In: Proceedings of the 10th International Conference on Geosynthetics. Berlin, Germany.
- Iglesia, G.R., Einstein, H.H., Whitman, R.V., 2011. Validation of centrifuge model scaling for soil systems via trapdoor tests. *J. Geotech. Geoenviron. Eng.* 137 (11), 1075–1089.
- Jones, C.J.F.P., Cooper, A.H., 2005. Road construction over voids caused by active gypsum dissolution, with an example from Ripon, North Yorkshire, England. *Environ. Geol.* 48 (3), 384–394.
- Mair, R., Taylor, R., 1997. Bored tunnelling in the urban environment. In: Proceedings of the Fourteenth International Conference on Soil Mechanics and Foundation Engineering. Rotterdam, pp. 2353–2385.
- Mair, R.J., 2008. Tunnelling and geotechnics: new horizons. *Geotechnique* 58 (9), 695–736.
- Marshall, A.M., Farrell, R.P., Klar, A., Mair, R., 2012. Tunnels in sands: the effect of size, depth and volume loss on greenfield displacements. *Geotechnique* 62 (5), 385–399.
- Peck, R.B., 1969. Deep excavations and tunnelling in soft ground. In: 7th International Conference on Soil Mechanics and Foundation Engineering. Mexico City, Mexico, pp. 225–290.
- Pham, M.-T., Briçon, L., Dias, D., Abdelouhab, A., 2018. Investigation of load transfer mechanisms in granular platforms reinforced by geosynthetics above cavities. *Geotext. Geomembranes* 46 (5), 611–624.
- Potts, V.J., Zdravkovic, L., Dixon, N., 7 – 10 September 2008. Assessment of BS8006: 1995 design method for reinforced fill layers above voids. In: Proceedings of the 4th European Geosynthetics Conference. Edinburgh, United Kingdom..
- SANS 1936-1, 2012. Development of Dolomite Land: Part 1. Tech. Rep. South African National Standards.
- Schofield, A.N., 1980. Cambridge geotechnical centrifuge operations. *Geotechnique* 30 (3), 227–268.
- Springman, S.M., Bolton, M.D., Sharma, J., Balachandran, S., 11 – 13 November 1992. Modelling and instrumentation of a geotextile in the geotechnical centrifuge. In: Proceedings of the International Symposium on Earth Reinforcement Practice. Kyushu, Japan, pp. 167–172.
- Stanier, S., Blaber, J., Take, W.A., White, D., 2015. Improved image-based deformation measurement for geotechnical applications. *Can. Geotech. J.* 53 (5), 727–739.
- Taylor, R.N., 1995. *Geotechnical Centrifuge Technology*. Blackie Academic and Professional, Glasgow.
- van Eekelen, S.J.M., Bezuijen, A., 2012. Model experiments on geosynthetic reinforced piled embankments, 3D test series. In: Proceedings of the 2nd European Conference on Physical Modelling in Geotechnics. Delft, Netherlands.
- van Eekelen, S.J.M., Bezuijen, A., Lodder, H.J., van Tol, A.F., 2012a. Model experiments on piled embankments. Part I. *Geotext. Geomembranes* 32, 69–81.
- van Eekelen, S.J.M., Bezuijen, A., Lodder, H.J., van Tol, A.F., 2012b. Model experiments on piled embankments. Part II. *Geotext. Geomembranes* 32, 82–94.
- Villard, P., Briçon, L., 2008. Design of geosynthetic reinforcements for platforms subjected to localized sinkholes. *Can. Geotech. J.* 45 (2), 196–209.
- Villard, P., Gourc, J.P., Giraud, H., 2000. A geosynthetic reinforcement solution to prevent the formation of localized sinkholes. *Can. Geotech. J.* 37 (5), 987–999.
- Villard, P., Huckert, A., Briçon, L., 2016. Load transfer mechanisms in geotextile-reinforced embankments overlying voids: numerical approach and design. *Geotext. Geomembranes* 44 (3), 381–395.
- Viswanadham, B.V.S., König, D., 2004. Studies on scaling and instrumentation of a geogrid. *Geotext. Geomembranes* 22 (5), 307–328.
- Vorster, T.E., Klar, A., Soga, K., Mair, R.J., 2005. Estimating the effects of tunneling on existing pipelines. *J. Geotech. Geoenviron. Eng.* 131 (11), 1399–1410.
- Zhao, Y., Gafar, K., Elshafie, M.Z.E.B., Deeks, A.D., Knappett, J.A., Madabhushi, S.P.G., 4 – 6 August 2006. Calibration and use of a new automatic sand pourer. In: Proceedings of the 6th International Conference on Physical Modelling in Geotechnics. Hong Kong, pp. 265–270.